Received: 8 February 2021 | Revised: 14 June 2021 | Accepted: 29 June 2021

DOI: 10.1002/jbm.a.37266

RESEARCH ARTICLE

Society For Biomaterials | WILEY

Nanophase surface arrays on poly (lactic-co-glycolic acid) upregulate neural cell functions

Didem Mimiroglu[1,2] | Tulin Yanik[1,3] | Batur Ercan[4,5]

[1]Biochemistry, Graduate School of Natural and Applied Science, Middle East Technical University, Ankara, Turkey

[2]Biochemistry, Faculty of Science, Sivas Cumhuriyet University, Sivas, Turkey

[3]Department of Biological Sciences, Middle East Technical University, Ankara, Turkey

[4]Department of Metallurgical and Materials Engineering, Middle East Technical University, Ankara, Turkey

[5]BIOMATEN, Center of Excellence in Biomaterials and Tissue Engineering, Middle East Technical University, Ankara, Turkey

Correspondence
Batur Ercan, Department of Metallurgical and Materials Engineering, Middle East Technical University, 06800 Çankaya, Ankara, Turkey.
Email: baercan@metu.edu.tr

Funding information
The Young Scientist Award Programme (GEBIP) of the Turkish Academy of Sciences; The Young Scientist Awards Programme (BAGEP) of The Science Academy; The Scientific and Technological Research Council of Turkey, Grant/Award Number: 217M952

Abstract

Nerve guidance channels (NGCs) promote cell-extracellular matrix (ECM) interactions occurring within the nanoscale. However, studies focusing on the effects of nanophase topography on neural cell functions are limited, and mostly concentrated on the sub-micron level (>100 nm) surface topography. Therefore, the aim of this study was to fabricate <100 nm sized structures on poly lactic-co-glycolic acid (PLGA) films used in NGC applications to assess the effects of nanophase topography on neural cell functions. For this purpose, nanopit surface arrays were fabricated on PLGA surfaces via replica molding method. The results showed that neural cell proliferation increased up to 65% and c-fos protein expression increased up to 76% on PLGA surfaces having nanophase surface arrays compared to the control samples. It was observed that neural cells spread to a greater extend and formed more neurite extensions on the nanoarrayed surfaces compared to the control samples. These results were correlated with increased hydrophilicity and roughness of the nanophase PLGA surfaces, and point toward the promise of using nanoarrayed surfaces in NGC applications.

KEYWORDS
materials science, nanostructure, neural cells, PLGA, surface topography

1 | INTRODUCTION

Injuries in the peripheral nervous system (PNS) is one of the major public health problems in the worldwide.[1] In the United States alone, there are nearly 20 million people suffering from PNS injuries caused by trauma (i.e., traffic accidents, natural disasters, etc.) and various medical conditions, while there are nearly 300.000 people affected by it each year in Europe.[2,3] Though PNS can recover itself to a certain extent, there is variability in the regeneration process depending on the patient's overall health, as well as, type, size, and location of the injury. In fact, patients suffering from PNS injuries can wait for years for some level of recovery and, at the end, may be left with devastating sensory and motor deficits, which renders them disabled.[4]

There are various treatment options for PNS injuries. Autografting, allografting, and xenografting are among the commonly used treatments for PNS injuries larger than 1.5–3 cm.[3,5,6] However, these treatment options all have their drawbacks. Autografting, which is the gold-standard treatment for PNS injuries, requires the sacrifice of a donor nerve and can lead to donor site morbidity, pain, and neuroma. The limited availability of autografts is also problematic for severe nerve injuries requiring grafting to multiple anatomical locations. For the case of allografts, there are not sufficient number of available donors, while allografts and xenografts can both induce immune response in the recipients and can potentially lead to disease transmission form the donors to the recipients.[6] These complications limited the use of autografts, allografts, and xenografts and led to the development of nerve guidance channels (NGCs) for the treatment of PNS injuries. NGCs are tubular shaped hollow structures bridging the distal and proximal stumps of injured neurons.[3] The ends of the injured nerve stumps can be affixed into the ends of the tube and provides an isolated pathway conducive to regeneration.[7] NGCs direct axons sprouting from the proximal nerve stump, provide a

conduit for the diffusion of growth factors secreted by the injured nerve ends and reduce the infiltration of scar tissue.[8] There are various studies in literature investigating the use of biocompatible and biodegradable materials for NGC applications, such as polyvinilidene fluoride-trifluoroethylene (PVDF-TrFE), polycaprolactone (PCL), poly (ethylene glycol) (PEG), poly (lactic acid) (PLA), type I collagen, polyvinyl alcohol (PVA), and poly (lactic-co-glycolic acid) (PLGA).[9-12] In fact, the use of these materials as NGCs enhanced neural cell functions in vitro and translated into improved motor functions in vivo. For instance, Bini et al. tested PLGA based microbraided NGCs for sciatic nerve injury in rats and showed successful nerve regeneration after 1 month of implantation.[13] Though most results in literature highlighted the effectiveness and potential use of NGCs for PNS injuries, the results were less than ideal where the use of NGCs could not secure full recovery for all test subjects. In fact, the rate and extent of recovery was observed to be worse than autologous grafts in some studies.[14] Clearly, revised strategies are required for the fabrication NGCs to be effective in PNS regeneration.

Neural cells interface with a variety of cell types in their natural niche, which possess surface topographies in the micron and nanometer range that stimulate and have a positive impact on neural cells functions.[15] In addition, the extracellular matrix (ECM) surrounding neural cells also possesses nanophase surface arrays and has building blocks that have dimensions within nanometer regime. For instance, peripheral nerves embedded inside endonerium contain different types collagen molecules (the collagen is about 1.5 nm thickness and 300 nm long rod-shaped molecules[16]), while the basal lamina in endoneurium that surrounds Schwann cells is composed of various molecules including fibronectin (the width of fibronectin protein is approximately 3 nm[17]) and heparan sulfate proteoglycan (has a protein core of 80 nm[18]) that have nanometer dimensions. Considering the nanometer size range of molecules and the concomitant nanophase surface topography of ECM interacting with neural cells, fabrication of neural guidance channels that possess nanophase surface topography would allow neural cells to interact with a surface that mimic their natural niche. As a matter of fact, design of implant surfaces to mimic the nanoarray size of tissues has been investigated in various biomaterial applications, including orthopedic implants where fabrication of a nanoarrayed surface topography on PLGA surfaces to mimic the inorganic component of bone tissue was observed to upregulate adhesion, proliferation, and cellular functions of osteoblasts.[19]

In the last decade, neural cell functions on topographical structures were investigated in detail where most studies focused on the interactions between neural cells and biomaterial surfaces to have "micron" and "submicron" scale topography.[20] For instance, neural stem cells expressed longer extensions on PLGA surfaces that had 400 nm grooves compared to smooth surfaces independent of the presence of 3,4-dihydroxy-L-phenilalanin (DOPA) coating.[21] In a different study, astrocytic scar tissue formation upon the changes in nanophase topographical array size of anodic aluminum oxide (AAO) was investigated to optimize biological interactions for neural electrode applications. The results showed that astrocyte adhesion was higher onto surfaces with small porous structures (~20 nm) compared to the ones having larger pores (~90 nm).[22] In addition, astrocytes expressed more focal adhesions on AAO surfaces having smaller pore size.[22] Though the authors focused on the effect of surface array dimensions less than 100 nm, the material of investigation was porous aluminum oxide and astrocytes were used to investigate the efficacy of AAO for neural electrodes.

Though there are multiple studies investigating the effect of submicron (>1 μm) and micron sized topographical structures for NGC applications, studies focusing on the effect of surface array size less than 100 nm is very limited. For optimal neural regeneration, it is essential to understand neural cell functions upon their interaction with nanophase topographies having less than 100 nm (nanoscale) lateral array size. Herein, the influence of nanophase surface arrays fabricated on PLGA films, an American Food and Drug Administration (FDA) approved material used in NGC applications, was investigated to identify an optimal nanophase surface topography using N2a cell line (mouse neuroblastoma cells) for neural-tissue engineering applications. To understand the effect of nanophase surface topography on neural cell functions, 316L stainless steel (316L SS) surfaces having different sized nanopits were fabricated by anodization and these surfaces were used as molds to cast PLGA solution and to transfer their nanophase surface topography onto PLGA. Scanning electron microscopy, atomic force microscopy, X-ray photoelectron spectroscopy, Fourier-Transform Infrared Spectroscopy, and sessile drop water contact angle measurements were used to characterize surface morphology, topography, chemistry, and hydrophobicity, respectively. Cellular proliferation, morphology, and activity were evaluated to understand interaction of neural cells with nanophase PLGA surfaces.

2 | MATERIALS AND METHODS

2.1 | Materials

PURASORB® poly (lactic-co-glycolic acid) (w/w, 50:50) was provided by Corbion Purac (Amsterdam, The Netherlands). 3–4,5-dimethylthiazolyl-2,5-diphenyltetrazolium bromide (MTT), 4′,6-diamino-2-phenylindole (DAPI), hexamethyldisilazane, and bovine serum albumine (BSA) were purchased from Sigma-Aldrich (Germany). Cytopainter Staining Kit (ab112127), anti-vinculin primary antibody (ab129002, rabbit monoclonal), Alexa Fluor 488 secondary antibody (ab150077, goat anti-rabbit), anti-c-fos primary antibody (ab222699, rabbit) and peroxidase linked secondary antibody (ab6721, goat anti-rabbit IgG) were purchased from Abcam (Cambridge, UK). β-actin primary antibody (PA1183, rabbit), M-PER™ Mammalian Protein Extraction Reagent and Pierce™ Coomassie Protein Assay Kit were purchased from Thermo Fisher Scientific (Massachusetts, USA). Clarity™ Western ECL Substrate was purchased from Bio-Rad Laboratories (USA). Protease inhibitor cocktail tablets (Roche Complete Mini EDTA-free) were purchased from Roche Diagnostic Gmbh (Germany). Dithiothreitol (DTT) was purchased from Thermo Fisher Scientific (MA, USA).

2.2 | Preparation of PLGA films with nanophase topographies

PLGA films having nanophase surface topographies were fabricated utilizing anodized 316L SS surfaces as casting molds. To fabricate the molds, first, 316L SS foil (thickness 0.5 mm) was cut into 2.5 × 2.5 cm squares, followed by cleaning in acetone, 70% ethanol and ultrapure water each for 15 minutes (min), respectively. To obtain nanophase topography on 316L SS surfaces, the surface cleaned samples were anodized. For the anodization process, 5% (v/v) perchloric acid in ethylene glycol solution was used as an electrolyte and the temperature of the system was kept between 0 and 10°C range. A platinum mesh was used as the cathode and the 316L SS sample was the anode. 316L SS samples were anodized under 35 V for 5 min and 50 V for 6 min to obtain nanopit surface morphologies having different array sizes.[23] The anodized 316L SS samples were washed with ultrapure water and dried at room temperature (RT).

Once 316L SS samples having nanopit surfaces were fabricated, they were used as molds to transfer their nanophase surface topographies onto PLGA films. PLGA (50:50, molar ratio) was dissolved in chloroform to obtain 8% (w/v) solution and poured onto anodized 316L SS. The PLGA solution poured onto 316L SS allowed to evaporate for 1 hr at RT and 48 hr inside an oven at 37°C to remove the chloroform.[24] Afterward, PLGA films were peeled from the anodized 316L SS surfaces. PLGA films poured onto nonanodized 316L SS surfaces were used as control samples.

2.3 | Surface characterization

Scanning electron microscopy (SEM, FEI, NovaNano 430, Brno, The Czech Republic) was used to characterize the surface morphology of anodized 316L SS and PLGA film surfaces. Prior to imaging, PLGA samples were gold sputtered (Quorom SC7640 High Resolution Sputter Coater, Lewes, The UK) to obtain a conductive pathway on the sample surfaces. Twenty kilo volt potential was utilized to image 316L SS, while 5 kV was utilized for PLGA film surfaces.

2.4 | Surface topography measurements

Atomic force microscopy (AFM, Veeco Multimode V Atomic Force Microscopy, Santa Barbara, CA) was used to characterize surface topography of the samples. AFM was operated at the tapping mode and a silicone tip having 10 nm radius of curvature was used to obtain surface scans. 1 × 1 μm surface areas were scanned at 1 Hz scan rate. Scans were repeated in triplicate. AFM images were processed using Image Plus software (Peseux, Switzerland).

2.5 | Chemical analysis

PLGA film surfaces were characterized with X-ray photoelectron spectroscopy (XPS, PHI, 5000 Versa Probe, Minnesota, MN) to assess metal ion transfer from 316L SS molds. In XPS analysis, monochromatic Al K_α X-ray source was used with an approximate vacuum pressure of 7 Pa. Scans were collected from a spot diameter of 50 μm. Films were also characterized with Fourier-Transform Infrared Spectroscopy (FTIR, Perkim Elmer 400, Waltham, MA) to determine the presence of left-over solvent. FTIR analysis was completed using attenuated total reflection configuration with 4 cm^{-1} resolution in the 4,000–400 cm^{-1} range. Background spectra were subtracted from the obtained reflectance data and an average of 4 spectra was reported for each sample.

2.6 | Water contact angle analysis

Hydrophobicity of the samples were characterized with sessile drop water contact angle technique using a goniometer (EasyDrop, KRÜSS GmbH, Hamburg, Germany). Three micro liter ultrapure water was dropped onto PLGA film surfaces and the surface contact angles were measured after 10 s. Measurements were repeated in quadruplicate for each sample.

2.7 | Cell culture

A mouse neuroblastoma cell line, N2a (Neuro2-a, ATCC® CCL-131™), was used to test biological performance of the PLGA films in vitro due to the widespread use of this cell line in cytotoxicity assays.[25,26] N2a cells were cultured in Dulbecco's Modified Eagle Medium (DMEM) supplemented with 10% fetal bovine serum (FBS), 2 mM L-Glutamine, and 1% penicillin/streptomycin (PS) under standard cell culture conditions (5% CO_2, 37°C) as per established protocols.[27]

2.8 | Cellular proliferation

Prior to cell culture, PLGA films were cut into 6 mm diameter samples (~70 μm thick) and rinsed with sterile 1× phosphate buffer saline (PBS), 70% ethanol, and 1×PBS, respectively. Afterward, both sides of the samples were sterilized with UV light for 1 hr.[28]

To assess cellular proliferation, MTT assay was used. N2a cells were seeded onto the PLGA films at a density of 2 × 10^4 cell/cm^2. N2a cellular adhesion and proliferation were determined at 4 hr and 1, 3, and 5 days in vitro. At the end of the prescribed time periods, cells were treated with MTT solution (1 mg/ml, 100 μl/well) for 3 hr to form formazan crystals under standard cell culture conditions (5% CO_2, 37°C). Afterward, formazan crystals formed on PLGA films were dissolved using 0.1 N HCl solution prepared in isopropanol (100 μl/well). The absorbance values of the solutions containing dissolved formazan were recorded using Microplate Absorbance reader (Bio-rad, Hercules, CA) at 570 nm (reference wavelength-650 nm). The absorbance of the blank samples without any cells were subtracted from the obtained absorbance values. Cellular proliferation experiments were performed three times each with three replicates.

2.9 | Immunofluorescence imaging

The morphology of N2a cells was evaluated with fluorescence staining. Specifically, DAPI, anti-f-actin, and anti-vinculin staining procedures were applied to observe the nuclei, cellular morphologies and focal contact formations on each sample, respectively. N2a cells were seeded at density of 1×10^4 cell/cm^2 onto the PLGA films and incubated for 72 hr. At the end of 72 hr, cells were fixed with 4% paraformaldehyde solution for 30 min at RT. Once 4% paraformaldehyde solutions were discarded, the fixed cells were rinsed with 1X PBS and cell membranes were permeated with 0.2% Triton X-100 for 30 min. 5% BSA in 1×PBS was used as a blocking solution. 0.5% BSA in 1×PBS was used to dilute primary and secondary antibodies. Blocking step was applied prior to and after the incorporation of primary antibody solution. For the antibody staining procedure, the permeated cells were initially incubated with anti-vinculin primary antibody (rabbit monoclonal, 1:200) for 90 min, followed by rinsing with 1xPBS. Afterward, the cells were incubated with Alexa Flour 488 conjugated secondary antibody (goat anti-rabbit IgG, 1:1,000) and rhodamine-phalloidin for 1 hr. Cells were also stained with DAPI (0.5% BSA in 1×PBS, 1:40,000) 30 min to image their nuclei. Confocal microscopy (Zeiss LSM800, Germany) was used for imaging and the captured images were merged with ZEISS ZEN Imaging Software (Jena, Germany). Images were quantitatively analyzed using ImageJ (NIH, USA). Immunofluorescence staining experiments were repeated in triplicate.

2.10 | SEM imaging

In addition to immunofluorescence imaging, the morphology of the N2a cells was also evaluated with SEM imaging. Prior to SEM imaging, N2a cells were seeded at density of 1×10^4 cell/cm^2 onto the PLGA films and incubated for 24 hr. At the end of 24 hr, cells were fixed with 4% paraformaldehyde solution for 20 min at RT. Once paraformaldehyde solution was discarded, the fixed cells were rinsed with 1X PBS and dried gradually using 30, 70, 90, and 100% ethanol solutions, respectively. Afterward, cells were incubated with hexamethyldisilazane for 12 hr at RT for final drying. Prior to imaging, cells were sputter coated with gold (Quorom SC7640 High Resolution Sputter Coater, Lewes, UK) to obtain a conductive pathway on the samples. SEM micrographs of N2a cells were used to count number of neural cell extensions. The number of neurite extensions were normalized by dividing neurite extension number to cellular count for control, P-30 and P-80 groups ($n = 7$).[29,30]

2.11 | Neuronal cell activity

The c-fos protein expression levels were assessed with Western blotting to identify N2a cellular activity. First, N2a cells were seeded onto PLGA films at a density of 5×10^4 cell/cm^2 and incubated for 48 hr ($n = 3$). After the incubation, cells were lysed using a buffer solution (M-PER™ Mammalian Protein Extraction Reagent) plus protease inhibitors, followed by centrifuging at 13.000 rpm for 10 min. The supernatant was assayed for protein content with Bradford assay, while 10 μg of protein from each extract were analyzed with Western blot.[31] Afterward, the nitrocellulose membrane blots were probed with anti-c-fos (rabbit, 5% milk in phosphate buffer, 1:1,000) overnight at 4°C. Same procedure was repeated for β-actin secondary antibody (rabbit, 5% milk in phosphate buffer, 1:1,500) as a loading control. Western blot signal was enhanced by chemiluminescence using goat antirabbit IgG coupled to horseradish peroxidase (5% milk in phosphate buffer, 1:10,000) as the secondary antibody using a gel imaging system (BIO-RAD ChemiDoc MP Imaging System). The protein band intensities were quantified with the ImageJ software (NIH, MD). Experiments were repeated in triplicate.

2.12 | Protein adsorption on PLGA film surfaces assay

Protein adsorption assay was used based on previously established protocols.[32] Briefly, 1×1 cm PLGA films were UV sterilized and placed separately inside the wells of tissue culture plate. DMEM medium containing 10% FBS (1 ml) was added onto each sample and incubated for 4 hr under standard cell culture conditions (5% CO_2, 37°C). At the end of incubation, DMEM medium was discarded and each sample was rinsed with 1xPBS. Afterward, samples were transferred to a fresh well and 300 μl protein removal buffer solution (8 M urea, 0.1 M TrisBase, and 0.01 M DTT, adjusted pH 8.6) was added onto each sample. The samples were incubated inside the protein buffer solution for 20 min on a shaker at 40 rpm. After elution of the adsorbed proteins, the protein concentration was assayed using Bradford assay.[33] Experiments were repeated in triplicate.

2.13 | Statistical analysis

The Shapiro–Wilk test was applied to verify the normality of the results (IBM SPSS Statistics, Version 25), followed by analyzing for statistical significance using ANOVA (IBM SPSS Statistics, Version 25). Statistical significance was defined as a p <.05. The values were given as mean ± standard deviation (SD).

3 | RESULTS

SEM micrographs of anodized 316L SS samples were given in Figure 1. The anodization process formed nanopit structures homogenously across the 316L SS surfaces. Nanopits having two different diameters (lateral) were fabricated on 316L SS surfaces by altering the anodization conditions where anodizing at 35 V for 5 min formed 32 ± 1 nm and 50 V for 6 min formed 79 ± 1 nm sized nanopits, respectively (Figure 1b,c). Anodized 316L SS samples were used to obtain nanophase topographies on PLGA films via the replica molding process where 8% PLGA was poured onto the anodized 316L SS

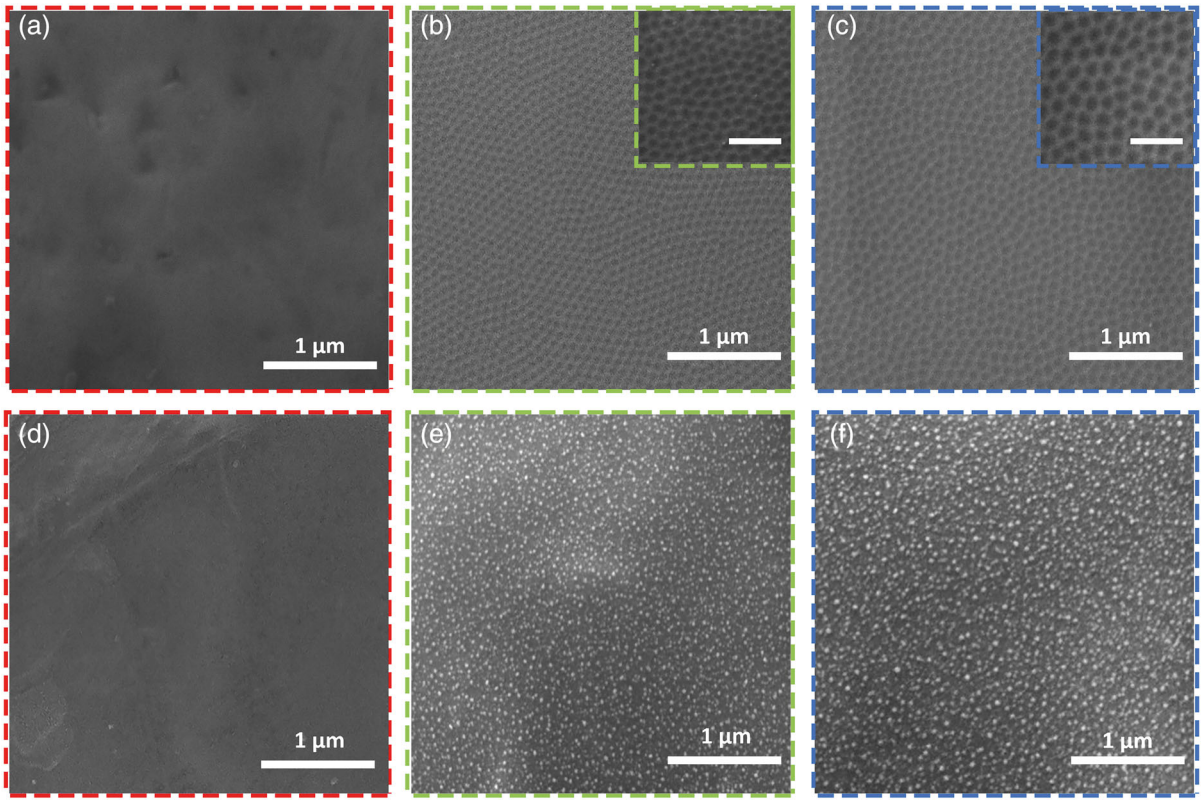

FIGURE 1 SEM micrographs of (a) control, (b) A-30 and (c) A-80, (d) control, (e) P-30 and (f) P-80 samples. The scale bars of insets are 3 μm

TABLE 1 The abbreviations used for different sample types

Sample	Abbreviation for anodized steel	Abbreviation for PLGA replica
Nonanodized	Control	Control
Anodized surfaces having 32 ± 1 nm pits	A-30	P-30
Anodized surfaces having 79 ± 1 nm pits	A-80	P-80

surfaces, followed by evaporation of the solvent and peeling of PLGA from the anodized 316 L SS surfaces. 316L SS samples having 32 ± 1 nm and 79 ± 1 nm array size will be referred as "A-30" and "A-80 nm," respectively; and the PLGA films peeled from A-30 and A-80 will be referred as "P-30" and "P-80", respectively (Table 1).

While the control samples molded onto nonanodized 316L SS (Figure 1d) did not have an array of periodically repeating surface arrays, P-30 and P-80 samples displayed nanoarrays resembling the topography of anodized 316L SS surfaces (Figure 1e,f). SEM images confirmed successful transfer of nanopatterns from 316L SS surfaces onto the PLGA films. Since while PLGA surfaces with nanoarrays were deteriorated due to high magnification (with electron beam) during the SEM analysis, P-30 and P-80 sample surfaces were not seen as bumpy as AFM micrographs (Figure 2). It was important to note that there was no cracking or damage during peeling of the PLGA films from the anodized 316L SS. These results were in-line with literature findings where nanophase surface topographies were successfully transferred from AAO templates onto PLGA films.[34]

2D and 3D AFM micrographs and height profiles obtained from the PLGA samples were displayed in Figure 2. AFM micrographs further confirm successful molding of bumpy nanophase surface arrays onto the PLGA films. Height profile analysis provided information on the size of surface arrays on the PLGA films. The sizes of individual bumps were measured to be 29.4 ± 3.1 and 80.2 ± 3.5 nm for P-30 and P-80, respectively, and heights of individual bumps were measured to be 1.9 ± 0.1 and 4.1 ± 0.2 nm for P-30 and P-80, respectively (Figure 2). The dimensions of nanophase bumps on PLGA surfaces matched the array size of nanopits obtained on anodized 316L SS surfaces. The root-mean square roughness values (S_q) calculated from the scans were 1.23 ± 0.05, 1.85 ± 0.05, and 4.52 ± 0.15 nm for the control, P-30, and P-80, respectively (Table 2). The arithmetical mean square roughness values (S_a) calculated from the scans were 0.99 ± 0.04, 1.50 ± 0.03, and 3.73 ± 0.13 nm for the control, P-30, and P-80, respectively (Table 2). The S_q and S_a values for P-30 and P-80 were both higher compared to the control samples (p <.001). The obtained differences in surface roughness values were expected and in-line with the principles of anodization. Specifically, during anodization process 316L SS surfaces were polished to a near mirror finish and all surface extremities, including grain boundaries, were removed from the anodized surfaces. Having this said, aside from polishing and smoothing out large surface asperities, anodization process also formed nanopit arrays on 316L SS surfaces. Upon molding of PLGA

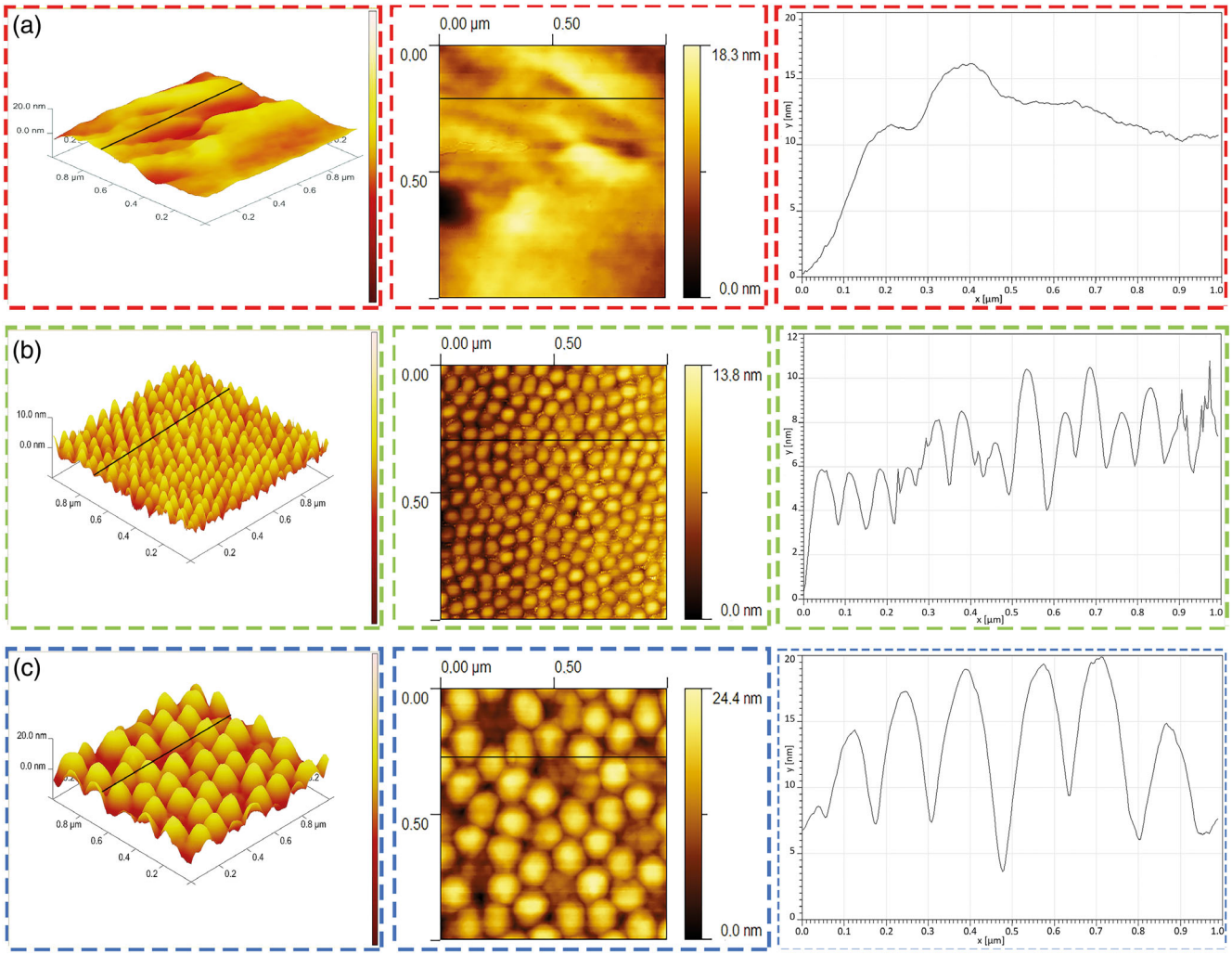

FIGURE 2 AFM images for (a) control, (b) P-30, (c) P-80 samples showing 3D (left) and 2D (middle) micrographs, and height profiles (right). The thick black lines on 2D AFM micrographs indicate where height profiles were obtained on the PLGA films

TABLE 2 Values for root mean square roughness, average roughness, and surface area

Sample	Root mean square surface roughness (S_q, nm)	Arithmetical mean surface roughness (S_a, nm)	Surface area (µm^2)
Control	1.23 ± 0.05	0.99 ± 0.04	1.003 ± 0.001
P-30	1.85 ± 0.05**	1.50 ± 0.03**	1.016 ± 0.001**
P-80	4.52 ± 0.15**	3.73 ± 0.13**	1.021 ± 0.001**

Note: Values are mean ± *SD*.
**p <.001.

onto the anodized 316L surfaces, arrays of nanophase bumps formed on PLGA, which led to an increase in S_q and S_a values. In this study, surface areas were measured to be 1.003 ± 0.001, 1.016 ± 0.001, and 1.021 ± 0.001 µm^2 for control, P-30, and P-80 samples, respectively. Though the increase in surface areas for P-30 and P- 80 were minor, they were found to be statistically significant compared to the control (p <.001). During anodization process, polishing of surface asperities and formation of nanopits on 316L SS were taking place simultaneously, where the former one was decreasing, yet, the latter one was increasing the total surface area. PLGA films having nanophase surface topographies were characterized with XPS and FTIR for chemical analysis (Figures 3a and S1). It was important to note that PLGA films peeled from the anodized 316L SS surfaces did not express Fe, Cr, Ni, and Mo peaks in their XPS spectra (Figure 3a) indicating that the oxide layer did not delaminate from the anodized 316L SS surfaces and stick to PLGA films during replica molding process.[35] Interestingly, XPS results revealed presence of trace silicon on PLGA films. Specifically, 3.2, 2.2, and 1.5% silicon were observed for control, P-30, and P-80 surfaces. It can be speculated that the use of glassware during specimen fabrication led to silicon contamination on the surfaces.

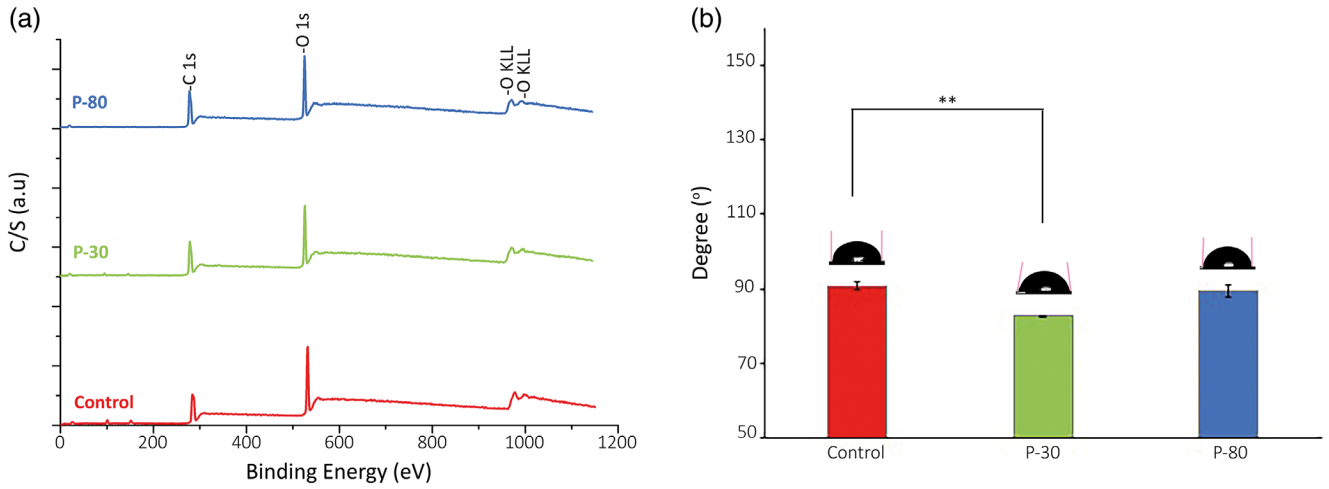

FIGURE 3 (a) XPS and (b) water contact angles for PLGA samples. Values are mean ± *SD*, $^{**}p < .001$

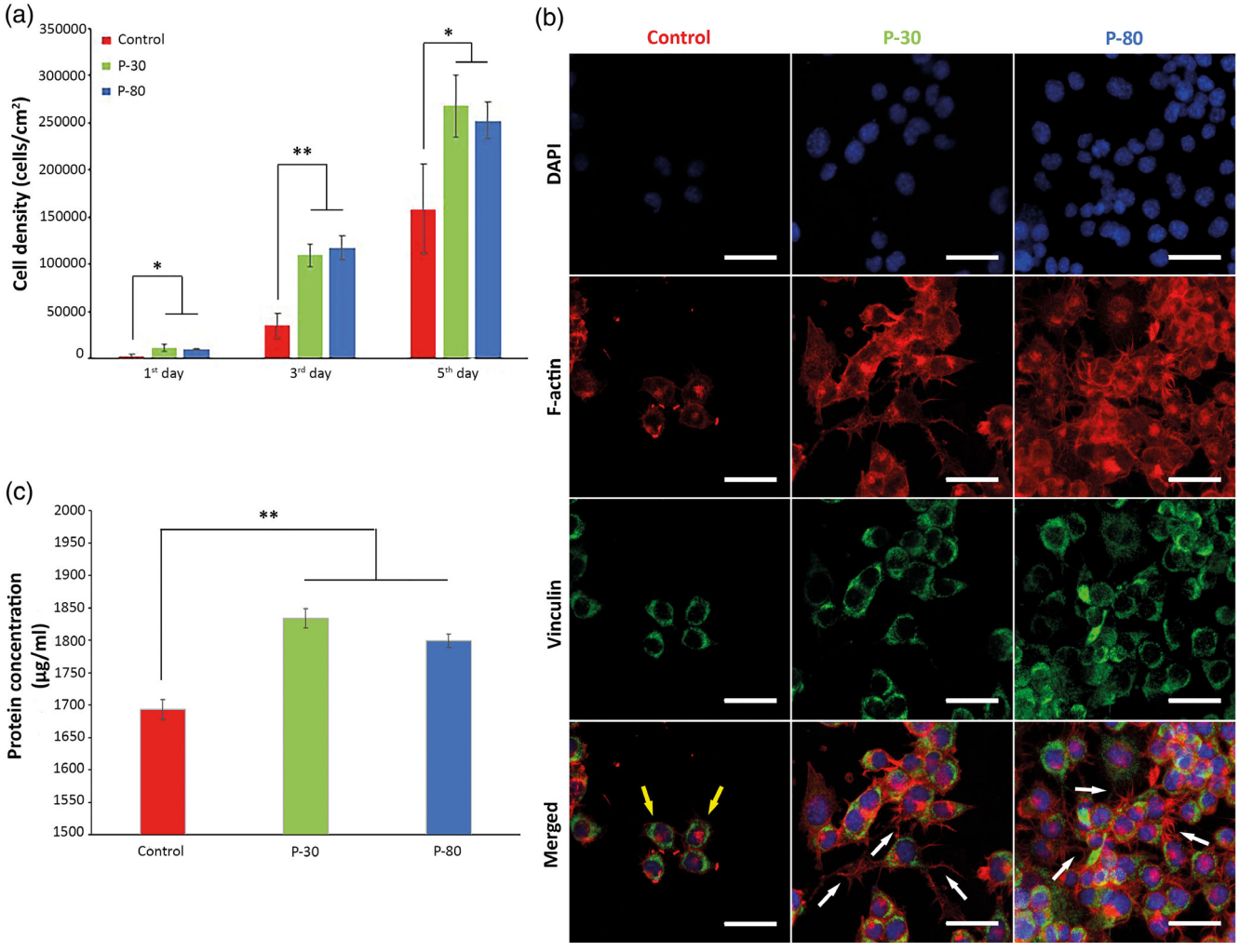

FIGURE 4 (a) N2a proliferation on control, P-30, and P-80 samples up to 5 days in vitro. Values are mean ± *SD* ($n = 3$), $^{*}p < .05$, $^{**}p < .01$. (b) The N2a cells stained with DAPI for nucleus (blue fluorescence, first row), phalloidin for f-actin (red fluorescence, second row) and Alexa-Fluor 488 for vinculin (green fluorescence, third row) on control, P-30, and P-80 samples after 72 hr incubation. Bottom row shows the merged images. Scale bars are 20 µm. (c) Protein adsorption results for control, P-30, and P-80 samples

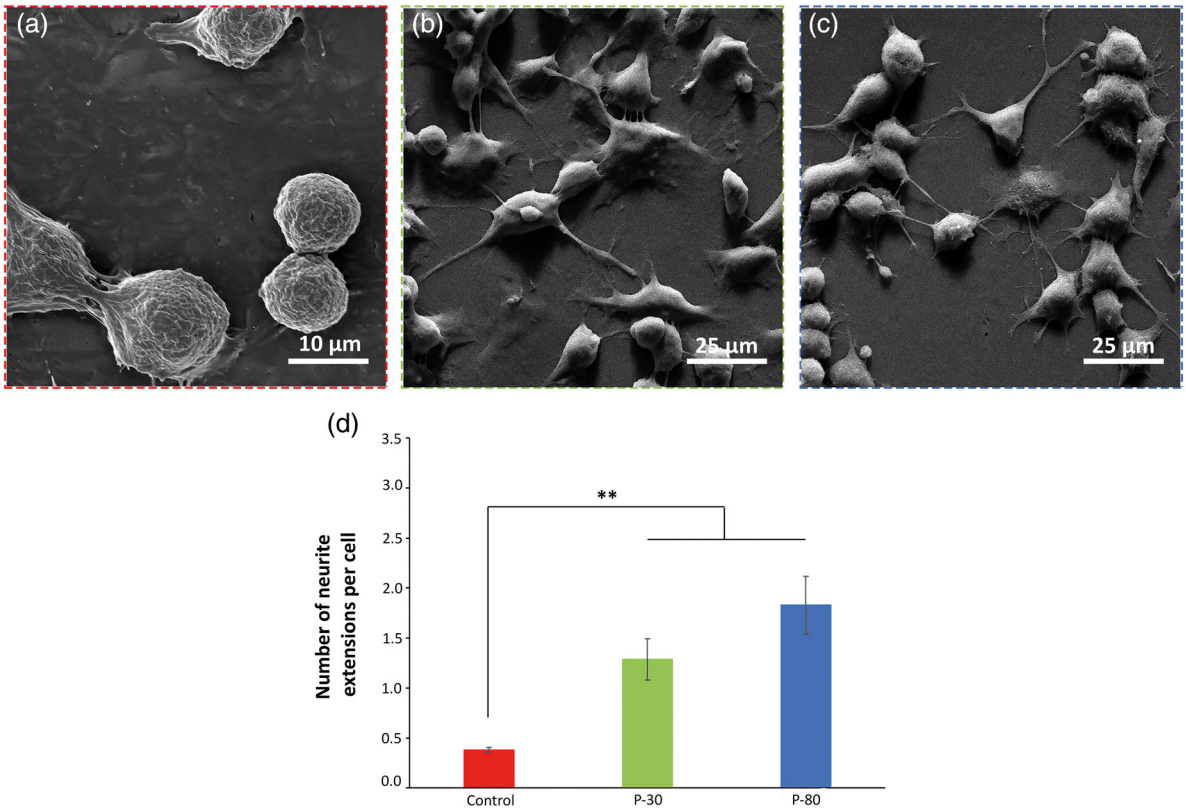

FIGURE 5 SEM images of N2a cells on (a) control, (b) P-30, and (c) P-80 samples. d) Number of neurite extension per cell for the control, P-30, and P-80 samples. The values are mean ± *SD*, $n = 7$, $^{*}p < .01$

FTIR spectra of the PLGA samples revealed characteristic C—H (2,850 cm^{-1}), C═O (1,747 cm^{-1}), CH_3 (1,383 cm^{-1}), and CH_2 (750 cm^{-1}) absorption bands that belong to PLGA film surfaces.[36,37] It was important to note there were no Cl peaks in the XPS or FTIR spectra of PLGA that would indicate the presence of left-over chloroform in this study. Chloroform was used to dissolve the PLGA polymer during replica molding and our results confirm successful removal of chloroform from the PLGA film surfaces.

Sessile drop water contact angles for the control, P-30, and P-80 groups were measured as 90.8° ± 1.1°, 82.7° ± 0.2°, and 89.4° ± 1.7°, respectively (Figure 3b). P-30 samples expressed lower water contact angle compared to the control samples ($p < .001$) and exhibited hydrophilic characteristics ($\theta < 90°$). However, there were no statistical difference between control and P-80 samples. The small decrease in the water contact angle of P-30 could be attributed to the presence of silicon on the surfaces, which was stated in the results for XPS analysis.

N2a cellular density at 4 hr (adhesion) and 1st, 3rd, and 5th day time points (proliferation) were shown in Figures S2 and 4a. N2a cell densities did not reveal any significant difference between the samples at 4 hr, indicating that cellular adhesion was similar onto all surfaces independent of the surface topography. Having this said, N2a cells proliferated on all samples and cellular densities on control, P-30, and P-80 increased up to 5 days of culture. At the 1st day in vitro, P-30 and P-80 samples had higher cellular density compared to the control samples ($p < .05$). At the 3rd day, N2a cellular densities were again higher on P-30 and P-80 compared to the control samples ($p < .01$). However, the differences in cellular densities between the nanophase samples and the control sample decreased at the 5th day of culture ($p < .05$). This was probably due to N2a cells reaching confluency on P-30 and P-80 samples that slowed down their proliferation rate (Figure 4a). On the other hand, cellular densities on P-30 and P-80 were similar at all investigated time points. These results showed that the increase in the cellular density between control and nanophase PLGA groups were due to increased cellular proliferation.

We explored focal adhesions, which are cellular sensing machinery of the cells. Focal adhesions are large macromolecular networks that facilitate communication between cells and their ECM, and vinculin is a part of focal adhesion macromolecule network. Thus, the recruitment of vinculin protein was investigated by immunofluorescence staining to visualize adhesion profile of N2a cells. N2a cells cultured on control, P-30, and P-80 surfaces were stained for their nuclei (blue), f-actin filaments (red), vinculin protein (green), and the images were displayed in Figure 4b. The merged immunofluorescence images (bottom row) qualitatively revealed that nanophase PLGA films had higher number of neural extensions (white arrows) and each of these neural extensions were longer than the control group (yellow arrows). Additionally, focal adhesions were observed to be distributed peripherally in all investigated samples. Cellular morphologies were

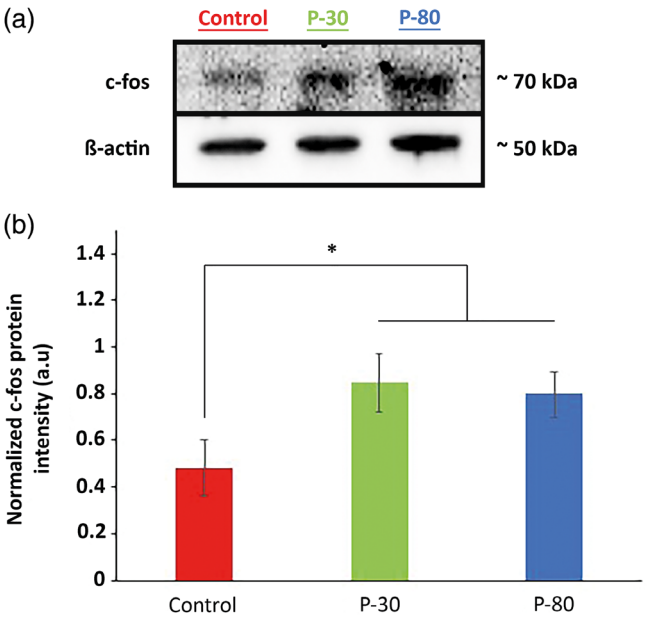

FIGURE 6 (a) Immunoblot images of control, P-30, and P-80 samples using anti-c-fos and anti-β-actin, (b) Western-blot analysis of c-fos protein in N2a cells cultured on control, P-30, and P-80 samples. The values are mean ± *SD*, $n = 3$, $^*p < .05$

also investigated using SEM and the captured images revealed that N2a cells expressed more neural extensions on P-30 and P-80 than the control samples ($p < .01$; Figure 5a–c). In fact, N2a cells had 0.38 ± 0.06, 1.29 ± 0.55, and 1.83 ± 0.76 neurite extensions per cell for the control P-30 and P-80 samples, respectively. However, no statistical significance in the number of neurite extensions per cell was detected between the P-30 and P-80 (Figure 5d). Clearly, cell-material interactions, which enhanced N2a proliferation and triggered the formation of focal adhesions and neural extensions, occurred at a higher extent on nanophase PLGA surfaces compared to the control surface.

It is well-known that cells interact with proteins adsorbed onto material surface, rather than directly interacting with the material itself.[38] In Figure 4c, it was observed that protein adsorption was significantly higher for P-30 and P-80 compared to control where 1,693.3 ± 27.2, 1,833.9 ± 25.8, and 1799.1 ± 18 μg/ml were found for the control, P-30, and P-80 samples, respectively. As a result of the protein adsorption profiles, N2a cells were adhering, proliferating and expressing more neural extension on P-30 and P-80 compared to control surfaces. In fact, these results were in-line with literature findings, where increase in density and functions of different cell types were associated with increased total protein adsorption, while increased protein adsorption was correlated with the increased surface roughness[38-40] For instance, TiO_2 surfaces having nanoleave morphology enhanced total serum protein adsorption onto its surfaces, which contributed to the increased endothelial cell viability compared to polished titanium. In addition, the dimensions of the nano-pores fabricated on poly(L-lactic acid) microfibers were found to enhance total protein adsorption, which was further correlated with cytocompatibility of these scaffolds to support vascular smooth muscle cell adhesion, proliferation, and expression of the vascular matrix proteins (elastin and collagen).[41,42]

C-fos protein has a key role in mitogen-activated protein kinase (MAPK) cascade mechanism, which maintains and controls the cellular proliferation, differentiation, and migration, and its expression is vital for firing neurons.[43] The c-fos expression levels were determined by Western blot to assess N2a cellular activity. As seen in Figure 6, the normalized intensity values for c-fos protein expressions were 0.48 ± 0.12, 0.85 ± 0.12, and 0.80 ± 0.10 (a.u) for the control, P-30, and P-80 samples, respectively. Western blot results showed that cells cultured on P-30 and P-80 films had higher c-fos protein expression compared to the control samples (Figure 6, $p < .05$). These results also confirmed that P-30 and P-80 enhanced N2a cellular functions compared to control samples.

4 | DISCUSSION

In NGC applications, surface modifications to induce topographical arrays have an important role in directing growth of axons between the damaged proximal and distal stumps. In our study, nanophase arrays having 30 and 80 nm lateral sizes were formed on PLGA films, which is a frequently used material in NGC applications, and the effect of surface nanophase topography on N2a cellular functions were investigated. The differences observed in N2a behavior on P-30 and P-80 films for the enhanced cellular functions suggested that cells sensed the subtle changes in the surface nanophase topography and reacted with a complex physiochemical response. This was in-line with previous findings where changes in nanophase surface topography altered cellular functions. For instance, altered array size on anodized surfaces independently allowed either augmented human mesenchymal stem cell adhesion when array size was ~30 nm or specific differentiation into osteoblasts when array size was ~70–100 nm.[44] In another study, human mesenchymal stem cells expressed well-spread cellular morphology with large focal adhesions on 15 and 55 nm high nanopillar surfaces compared to 100 nm high nanopillar surfaces.[45] Along the same line, electrospun fiber scaffolds with nanopits were shown to enhance interleukin-12 expression for M1 polarized macrophages compared to fibers having divots.[46,47] In this study, N2a cells had higher densities, higher number of neural extensions and up-regulated c-fos expression on P-30 and P-80 compared to the control samples. The reason for the enhanced N2a functions could be explained with changes in surface topography of PLGA films, where P-80 and P-30 surfaces had an array of nanophase surface features, which led to higher rms roughness values compared to the control samples. In fact, on gold surfaces having similar roughness values to the ones investigated in this study, neuronal cells had the lowest necrosis rate, expressed axonal outgrowth and functional cytoskeletal orientation, while increase in roughness to 80–100 nm led to disorganized focal adhesion complexes.[48] It was clear that N2a cells sensed the nanophase topography introduced onto P-30 and P-80 surfaces and responded by enhancing their proliferation and functions. Having this said, the lack of surface asperities removed from 316L SS during anodization, yet present on the control samples, could

have contributed to the promotion of cellular functions for P-30 and P-80 samples. In addition to the effect of surface topography, the increased hydrophilicity was known to dictate neural cell adhesion, proliferation and functions and focal adhesion expression.[22] Since P-30 was hydrophilic compared to the control sample, perhaps, increased hydrophilicity of P-30 could have a minor contribution for the observed differences in N2a cellular functions.[49,50] However, the changes in hydrophilicity could not account for the increased cellular function on P-80.

Since the total amount of proteins adsorbed onto the PLGA films increased upon surface modification, it could be speculated that the adsorption of cell adhesive serum proteins, that is, fibronectin and laminin, which were demonstrated to control adhesion, proliferation, and functions of anchorage dependent cells also increased.[51] In fact, the surface concentration and bioavailability of fibronectin and collagen type IV were shown to enhance on nanophase PLGA compared to its conventional counterpart.[24,52] It could be speculated that enhanced concentration of cell adhesive serum proteins on P-30 and P-80 surfaces could have contributed to the observed changes in the cellular functions of N2a cells.

To sum up, our results indicated that nanophase topographical arrays having lateral dimensions less than 100 nm may provide positive impacts on the proliferation and functions of neurons. Thus, fabrication of nanophase surface topographies should be investigated further for the next generation NGCs for PNS injuries.

5 | CONCLUSIONS

In this study, nanophase arrays having different sizes were fabricated on PLGA films via replica molding technique to investigate the effects of nanophase topographies on neural cell functions. For the replica molding process, 316L SS molds having different nanopit lateral diameters (32 ± 1 nm and 79 ± 0.5 nm) were used. The SEM and AFM analysis confirmed the successful transfer of nanophase topographies from the molds onto the PLGA films. XPS and FTIR analysis did not reveal presence of an oxide layer or left-over solvent for the PLGA films. Protein adsorption studies revealed enhanced adsorption of proteins onto nanophase PLGA compared to the control samples. Importantly, N2a cells cultured on nanophase PLGA films exhibited enhanced proliferation and higher number of neurite extensions, and at the same time, up-regulated c-fos protein expression compared to the ones cultured on the control samples. Cumulatively, the results revealed that fabrication of nanophase arrays on PLGA films could be promising for NGC applications.

ACKNOWLEDGMENTS

This work was financially supported by The Scientific and Technological Research Council of Turkey (Grant no: 217M952) and partially supported by The Young Scientist Awards Programme (BAGEP) of The Science Academy, Turkey and The Young Scientist Award Programme (GEBIP) of the Turkish Academy of Sciences. The authors would like to thank Corbion Purac (Amsterdam, The Netherlands) for providing PURASORB® poly (lactic-co-glycolic acid) (w/w, 50:50), BIOMATEN-METU Center of Excellence in Biomaterials and Tissue Engineering (BIOMATEN) for sessile drop water contact angle analysis and confocal microscopy analysis and Middle East Technical University (METU) Central Laboratory for FTIR, AFM, and XPS measurements.

CONFLICT OF INTEREST

The authors declare no potential conflict of interest.

DATA AVAILABILITY STATEMENT

Research data are not shared.

ORCID

Didem Mimiroglu https://orcid.org/0000-0003-2838-9719

Batur Ercan https://orcid.org/0000-0003-1657-1142

REFERENCES

1. Vela F, Martínez-Chacón G, Ballestín A, Campos J, Sánchez-Margallo F, Abellán E. Animal models used to study direct peripheral nerve repair: a systematic review. *Neural Regen Res*. 2020;*15*:491-502.
2. Quan Q, Meng HY, Chang B, et al. Aligned fibers enhance nerve guide conduits when bridging peripheral nerve defects focused on early repair stage. *Neural Regen Res*. 2019;*14*:903-912.
3. Houshyar S, Bhattacharyya A, Shanks R. Peripheral nerve conduit: materials and structures. *ACS Chem Neurosci*. 2019;*10*:3349-3365. https://doi.org/10.1021/acschemneuro.9b00203
4. Yang Y, Wang K, Gu X, Leong KW. Biophysical regulation of cell behavior—cross talk between substrate stiffness and nanotopography. *Engineering*. 2017;*3*:36-54. https://doi.org/10.1016/J.ENG.2017.01.014
5. Arslantunali D, Dursun T, Yucel D, Hasirci N, Hasirci V. Peripheral nerve conduits: technology update. *Med Devices Evid Res*. 2014;*7*:405-424.
6. Singh A, Shiekh PA, Das M, Seppälä J, Kumar A. Aligned chitosan-gelatin Cryogel-filled polyurethane nerve Guidance channel for neural tissue engineering: fabrication, characterization, and in vitro evaluation. *Biomacromolecules*. 2018;*20*:662-673.
7. Clements IP, Munson JM, Bellamkonda RV. Neuronal tissue engineering. *Biomater Science: an introduction to materials in medicine*. 2013;1291-1306. Oxford, UK: Elsevier.
8. Morelli S, Salerno S, Piscioneri A, Rende M, Campana C, De Bartolo L. Membrane approaches for liver and neuronal tissue engineering. *Compr Membr Sci Eng*. 2010;*3*:229-252.
9. Guo Z, Kofink S, Chen H, Liang J, Grijpma DW, Poot AA. Synthesis and characterization of rGO-graft-poly(trimethylene carbonate) for nerve regeneration conduits. *Biomed Mater*. 2019;*14*:034101.
10. Wu S, Chen M-S, Maurel P, Lee Y, Bunge MB, Arinzeh TL. Aligned fibrous PVDF-TrFE scaffolds with Schwann cells support neurite extension and myelination in vitro. *J Neural Eng*. 2018;*15*:056010.
11. Sharifi F, Patel BB, Dzuilko AK, Montazami R, Sakaguchi DS, Hashemi N. Polycaprolactone microfibrous scaffolds to navigate neural stem cells. *Biomacromolecules*. 2016;*17*:3287-3297.
12. Nectow AR, Marra KG, Kaplan DL. Biomaterials for the development of peripheral nerve guidance conduits. *Tissue Eng Part B Rev*. 2012;*18*:40-50. Available from http://www.ncbi.nlm.nih.gov/pmc/articles/PMC3262974/
13. Bini TB, Gao S, Xu X, Wang S, Ramakrishna S, Leong KW. Peripheral nerve regeneration by microbraided poly(L-lactide-co-glycolide) biodegradable polymer fibers. *J Biomed Mater Res - Part A*. 2004;*68*:286-295.

14. Luís AL, Rodrigues JM, Geuna S, et al. Use of PLGA 90:10 scaffolds enriched with in vitro-differentiated neural cells for repairing rat sciatic nerve defects. *Tissue Eng - Part A*. 2008;*14*:979-993.
15. Yang K, Yu SJ, Lee JS, et al. Electroconductive nanoscale topography for enhanced neuronal differentiation and electrophysiological maturation of human neural stem cells. *Nanoscale*. 2017;*9*:18737-18752.
16. Nelson DL, Cox MM. *Lehninger's Principles of Biochemistry*. New York: W H Free Co; 2013:1328.
17. Engel J, Odermatt E, Engel A, et al. Shapes, domain organizations and flexibility of laminin and fibronectin, two multifunctional proteins of the extracellular matrix. *J Mol Biol*. 1981;*150*:97-120.
18. Paulsson M, Yurchenco PD, Ruben GC, Engel J, Timpl R. Structure of low density heparan sulfate proteoglycan isolated from a mouse tumor basement membrane. *J Mol Biol*. 1987;*197*:297-313.
19. Torres-Lagares D, Castellanos-Cosano L, Serrera-Figallo MA, et al. In vitro and in vivo study of poly(lactic-co-glycolic) (PLGA)membranes treated with oxygen plasma and coated with nanostructured hydroxyapatite ultrathin films for guided bone regeneration processes. *Polymers (Basel)*. 2017;*9*:410.
20. Cangellaris OV, Gillette MU. Biomaterials for enhancing neuronal repair. *Front Mater*. 2018;*5*:1-8. https://doi.org/10.3389/fmats.2018.00021/full
21. Yang K, Park E, Lee JS, et al. Biodegradable nanotopography combined with neurotrophic signals enhances contact guidance and neuronal differentiation of human neural stem cells. *Macromol Biosci*. 2015;*15*:1348-1356.
22. Ganguly D, Johnson CDL, Gottipati MK, Rende D, Borca-Tasciuc DA, Gilbert RJ. Specific nanoporous geometries on anodized alumina surfaces influence astrocyte adhesion and glial Fibrillary acidic protein immunoreactivity levels. *ACS Biomater Sci Eng*. 2018;*4*:128-141.
23. Zhang B, Ni H, Chen R, et al. A two-step anodic method to fabricate self-organised nanopore arrays on stainless steel. *Appl Surf Sci*. 2015;*351*:1161-1168. https://doi.org/10.1016/j.apsusc.2015.06.083
24. Carpenter J, Khang D, Webster TJ. Nanometer polymer surface features: the influence on surface energy, protein adsorption and endothelial cell adhesion. *Nanotechnology*. 2008;*19*:505103.
25. LePage KT, Dickey RW, Gerwick WH, Jester EL, Murray TF. On the use of neuro-2a neuroblastoma cells versus intact neurons in primary culture for neurotoxicity studies. *Crit Rev Neurobiol*. 2005;*17*:27-50.
26. Salto R, Vílchez JD, Girón MD, et al. β-Hydroxy-β-methylbutyrate (HMB) promotes neurite outgrowth in Neuro2a cells. *PLoS One*. 2015;*10*:1-13.
27. Riboni L, Prinetti A, Bassi R, Caminiti A, Tettamanti G. A mediator role of ceramide in the regulation of neuroblastoma neuro2a cell differentiation. *J Biol Chem*. 1995;*270*:26868-26875.
28. Miller DC, Haberstroh KM, Webster TJ. PLGA nanometer surface features manipulate fibronectin interactions for improved vascular cell adhesion. *Wiley Intersci*. 2006;*81*:678-684.
29. Ronn LCB, Ralets I, Hartz BP, et al. A simple procedure for quantification of neurite outgrowth based on stereological principles. *J Neurosci Methods*. 2000;*100*:25-32.
30. Pemberton K, Mersman B, Xu F. Using ImageJ to assess neurite outgrowth in mammalian cell cultures: research data quantification exercises in undergraduate neuroscience lab. *J Undergrad Neurosci Educ*. 2018;*16*:A186-A194. Available from http://www.ncbi.nlm.nih.gov/pubmed/30057501%0Ahttp://www.pubmedcentral.nih.gov/articlerender.fcgi?artid=PMC6057772
31. Mahmood T, Yang P-C. Western blot: technique, theory, and trouble shooting. *N Am J Med Sci*. 2012;*4*:429-434. Available from http://www.najms.org/article.asp?issn=1947-2714
32. Yang D, Lü X, Hong Y, Xi T, Zhang D. The molecular mechanism of mediation of adsorbed serum proteins to endothelial cells adhesion and growth on biomaterials. *Biomaterials*. 2013;*34*:5747-5758. https://doi.org/10.1016/j.biomaterials.2013.04.028
33. Bradford MM. A rapid and sensitive method for the quantitation of microgram quantities of protein utilizing the principle of protein-dye binding. *Anal Biochem*. 1976;*72*:248-254.
34. Wang GJ, Lin YC, Li CW, Hsueh CC, Hsu SH, Hung HS. Fabrication of orderly nanostructured PLGA scaffolds using anodic aluminum oxide templates. *Biomed Microdevices*. 2009;*11*:843-850.
35. Ni S, Sun L, Ercan B, Liu L, Ziemer K, Webster TJ. A mechanism for the enhanced attachment and proliferation of fibroblasts on anodized 316L stainless steel with nano-pit arrays. *J Biomed Mater Res - Part B Appl Biomater*. 2014;*102*:1297-1303.
36. Coates J. Interpretation of infrared spectra, a practical approach. *Encycl of Analytical Chem*. 2000;10815-10837.
37. Movasaghi Z, Rehman S, Rehman IU. Fourier transform infrared (FTIR) spectroscopy of biological tissues. *Appl Spectrosc Rev*. 2008;*43*:134-179.
38. Ngandu Mpoyi E, Cantini M, Reynolds PM, Gadegaard N, Dalby MJ, Salmerón-Sánchez M. Protein adsorption as a key mediator in the nanotopographical control of cell behavior. *ACS Nano*. 2016;*10*:6638-6647.
39. Scopelliti PE, Borgonovo A, Indrieri M, et al. The effect of surface nanometre-scale morphology on protein adsorption. *PLoS One*. 2010;*5*:1-9.
40. Hou Y, Xie W, Yu L, et al. Surface roughness gradients reveal topography-specific mechanosensitive responses in human mesenchymal stem cells. *Small*. 2020;*16*:1905422.
41. Mohan CC, Sreerekha PR, Divyarani VV, Nair S, Chennazhi K, Menon D. Influence of titania nanotopography on human vascular cell functionality and its proliferation in vitro. *J Mater Chem*. 2012;*22*:1326-1340.
42. Zhou Q, Xie J, Bao M, et al. Engineering aligned electrospun PLLA microfibers with nano-porous surface nanotopography for modulating the responses of vascular smooth muscle cells. *J Mater Chem B*. 2015;*3*:4439-4450. https://doi.org/10.1039/C5TB00051C
43. Bullitt E. Expression of C-fos-like protein as a marker for neuronal activity following noxious stimulation in the rat. *J Comp Neurol*. 1990;*296*:517-530.
44. Oh S, Brammer KS, Li YS, et al. Stem cell fate dictated solely by altered nanotube dimension. *Proc Natl Acad Sci U S A*. 2009;*106*:2130-2135. Available from: http://www.ncbi.nlm.nih.gov/pubmed/19179282
45. Sjöström T, Dalby MJ, Hart A, Tare R, Oreffo ROC, Su B. Fabrication of pillar-like titania nanostructures on titanium and their interactions with human skeletal stem cells. *Acta Biomater*. 2009;*5*:1433-1441.
46. Castro-Raucci LMS, Francischini MS, Teixeira LN, et al. Titanium with nanotopography induces osteoblast differentiation by regulating endogenous bone morphogenetic protein expression and signaling pathway. *J Cell Biochem*. 2016;*117*:1718-1729.
47. Schaub NJ, D'Amato AR, Mason A, et al. The effect of engineered nanotopography of electrospun microfibers on fiber rigidity and macrophage cytokine production. *J Biomater Sci Polym Ed*. 2017;*28*:1303-1323. https://doi.org/10.1080/09205063.2017.1321345
48. Brunetti V, Maiorano G, Rizzello L, et al. Neurons sense nanoscale roughness with nanometer sensitivity. *Proc Natl Acad Sci U S A*. 2010;*107*:6264-6269.
49. Khorasani MT, Mirzadeh H, Irani S. Plasma surface modification of poly (l-lactic acid) and poly (lactic-co-glycolic acid) films for improvement of nerve cells adhesion. *Radiat Phys Chem*. 2008;*77*:280-287.
50. Sadeghi A, Moztarzadeh F, Aghazadeh MJ. Investigating the effect of chitosan on hydrophilicity and bioactivity of conductive electrospun composite scaffold for neural tissue engineering. *Int J Biol Macromol*. 2019;*121*:625-632. https://doi.org/10.1016/j.ijbiomac.2018.10.022
51. Ercan B, Khang D, Carpenter J, Webster TJ. Using mathematical models to understand the effect of nanoscale roughness on protein adsorption for improving medical devices. *Int J Nanomedicine*. 2013;*8*:75-81.

52. Li M, Mondrinos MJ, Chen X, Gandhi MR, Ko FK, Lelkes PI. Elastin blends for tissue engineering scaffolds. *J Biomed Mater Res Part A*. 2006;79:963-973. Available from: http://www.ncbi.nlm.nih.gov/pubmed/16948146

SUPPORTING INFORMATION

Additional supporting information may be found online in the Supporting Information section at the end of this article.

How to cite this article: Mimiroglu, D., Yanik, T., & Ercan, B. (2022). Nanophase surface arrays on poly (lactic-co-glycolic acid) upregulate neural cell functions. *Journal of Biomedical Materials Research Part A*, *110*(1), 64–75. https://doi.org/10.1002/jbm.a.37266